DOI: 10.1002/ejic.201001001

Crystal Structures and Physical Properties of Three New Manganese-Based Coordination Polymers with *p*-Biphenyldicarboxylic Acid Linkers

Mads R. V. Jørgensen,[a] Henrik F. Clausen,[a] Mogens Christensen,[a] Rasmus D. Poulsen,[a] Jacob Overgaard,[a] and Bo B. Iversen*[a]

Keywords: Metal-organic frameworks / Carboxylate ligands / Magnetic properties / X-ray diffraction

Solvothermal synthesis with manganese nitrate, *p*-biphenyldicarboxylic acid, and three different solvents resulted in three new metal–organic framework materials: $Mn(C_{14}H_8O_4)(C_3H_7NO)_{2/3}$ (**1**), $Mn_2(C_{14}H_8O_4)_{3/2}(CHO_2)$ (**2**), and $Mn_3(C_{14}H_8O_4)_3(C_4H_9NO)_4$ (**3**). Two of the syntheses gave multiphase products, but one resulted in a phase-pure product **2**. The crystal structures of **1** and **3** were solved by using conventional single-crystal X-ray diffraction, whereas the small crystal size of **2** made use of intense synchrotron radiation necessary. The crystal structure of **1** is composed of layers, which are only held together by van der Waals forces between the solvent of one layer and the framework of the adjacent layers, and the compound decomposes upon exposure to air. Structures **2** and **3** are 3D frameworks. Phase-pure compound **2** does not contain the expected solvent diethylformamide, but formic acid residues. Measurements of magnetization and heat capacity data show that **2** is a metastable material with irreversible phase transitions at 6.5 or 4.5 K. In the metastable state, **2** is antiferromagnetic. Compound **3** has two types of pores along the *b* axis, and solvent molecules occupy the channels. Minor disorder of the solvent molecule is observed in one of the channels.

Introduction

The field of coordination polymers (CPs) continues to evolve with rapid pace, and it maintains a central position in modern chemistry. A decade ago the interest exploded to a large extent driven by the excellent gas absorption properties observed in CPs (also known as metal–organic frameworks).[1] The application of CPs quickly expanded into areas such as catalysis,[2] chemical separation,[3] and recently negative thermal expansion has also been studied.[4] Our interest has focused on the magnetic properties of CPs. By using very accurate low-temperature single-crystal synchrotron X-ray diffraction data, we have reported experimental charge densities for a range of CPs by using the multipole model.[5] These studies, for example, provided an understanding of the superexchange mechanisms responsible for the magnetic ordering in the materials. One series of studies on CPs containing 1D manganese chains connected by deprotonated benzenedicarboxylic acid (BDC) linkers was particularly successful, as it experimentally established the electrostatic potential within the nanopores.[6] This is of considerable interest for prediction of the inclusion properties of these porous materials. As an extension of these studies we have carried out syntheses with similar reactants but where the BDC linker has been replaced by deprotonated *para*-biphenyldicarboxylic acid (H_2BPDC). Here we report on the synthesis, crystal structures, and physical properties of three new manganese-based CPs linked by BPDC: $Mn(C_{14}H_8O_4)(C_3H_7NO)_{2/3}$ (**1**), $Mn_2(C_{14}H_8O_4)_{3/2}(CHO_2)$ (**2**), and $Mn_3(C_{14}H_8O_4)_3(C_4H_9NO)_4$ (**3**). For **1** and **3** multiphase products were obtained, which excluded physical property characterization. However, for **2** a phase-pure product was obtained, and magnetic as well as thermal properties were measured. The crystals of **2** were so small that the structure could only be solved by using intense synchrotron radiation. A search in the Cambridge Structural Database for the BPDC linker and Mn atoms yielded three structures.[7] These, however, do not contain the same solvents as in this study but combinations of 1,10-phenanthroline, pyridine, piperazine, and water, and their crystal structures are therefore not directly comparable to the present structures.

Results and Discussion

Crystal Structure of 1

Crystallographic details for all the structures are given in Table 1. The structure of **1** consists of three-atom chains of manganese bridged by the delocalized carboxylate groups of the biphenyldicarboxylate (BPDC) linker (Figure 1). Neighboring Mn chains are connected through BPDC linkers, thus forming a continuous 2D layer with triangular shaped cavities (Figure 2). At the end of the Mn chains, a

[a] Centre for Materials Crystallography, Department of Chemistry and iNANO, Aarhus University,
8000 Århus C, Denmark
Fax: +45-8619-6199
E-mail: bo@chem.au.dk

Supporting information for this article is available on the WWW under http://dx.doi.org/10.1002/ejic.201001001.

Table 1. Crystallographic data for **1**, **2**, and **3**.

	$Mn(C_{14}H_8O_4)(C_3H_7NO)_{2/3}$ (**1**)	$Mn_2(C_{14}H_8O_4)_{3/2}(CHO_2)$ (**2**)	$Mn_3(C_{14}H_8O_4)_3(C_5H_{11}NO)_4$ (**3**)
Formula	$MnC_{16}H_{38/3}O_{14/3}N_{2/3}$	$Mn_2C_{22}H_{13}O_8$	$Mn_3C_{58}H_{60}O_{16}N_4$
Formula weight [g mol^{-1}]	343.87	515.20	1233.92
Crystal system	trigonal	monoclinic	monoclinic
Space group	$R\bar{3}$	$P2_1/c$	$P2_1/c$
T [K]	293(1)	120(1)	100(1)
Sample size [mm]^3	$100\times100\times150$	$40\times30\times140$	$100\times100\times100$
Z	9	4	4
a [Å]	14.020(2)	14.0014(30)	13.9444(3)
b [Å]	14.020(2)	14.4475(23)	18.1187(5)
c [Å]	19.893(4)	8.8943(11)	12.0758(3)
α [°]	90	90.000	90.000
β [°]	90	90.280(14)	112.894(1)
γ [°]	120	90.000	90.000
V [Å^3]	3386.2(10)	1799.2(5)	2810.66(12)
ρ [g cm^{-3}]	1.518	1.902	1.458
λ [Å]	0.71073	0.71000	0.71073
μ [mm^{-1}]	0.897	1.459	0.740
$\sin\theta/\lambda_{max}$ [Å^{-1}]	0.67	0.72	1.06
$N_{meas.}$, N_{unique}, $N_{2\sigma}$	9756, 1865, 937	19628, 5524, 5005	72643, 23362, 17496
R_{int}	0.0641	0.1037	0.0423
N_{var}	128	290	391
$R(F^2)_{2\sigma}$	0.0470	0.0781	0.0316
$R_w(F^2)_{2\sigma}$	0.0747	0.2014	0.0780
$R(F^2)_{all}$	0.1315	0.0874	0.0485
$R_w(F^2)_{all}$	0.092	0.2093	0.0824
S	0.893	1.147	0.930

DMF molecule coordinates directly to Mn2 through its oxygen (O10), and this DMF molecule is inherently disordered over three sites due to the existence of crystallographic threefold inversion symmetry. In the middle of the distinct Mn chain, which is aligned parallel to this threefold inversion axis, Mn1 is situated on an inversion center, resulting in a distorted octahedral coordination with angles varying by only ca. 5° from the ideal octahedron.

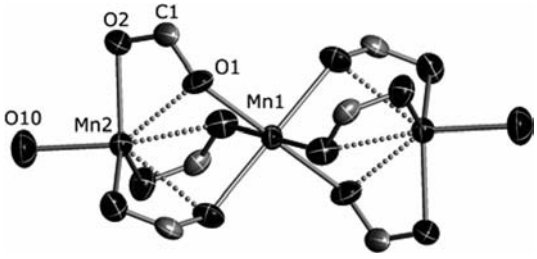

Figure 1. Three-atom manganese chain interconnected by the carboxylate groups of the BPDC linker of **1**. Questionable bonds are dotted. The thermal ellipsoids are shown at the 50% level.

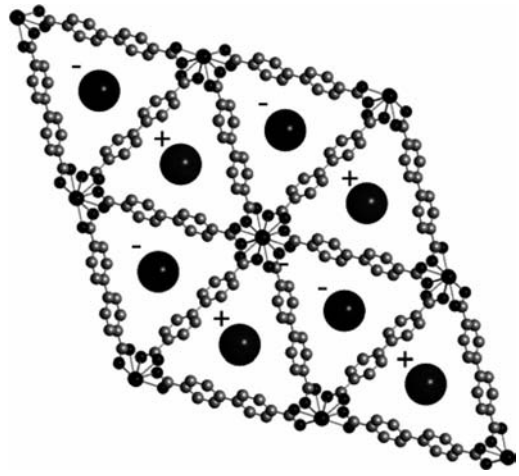

Figure 2. Layered structure viewed along the c axis of the unit cell. Spheres marked with a "+" represent the DMF molecules from the layer above and spheres marked with a "–" represent the DMF molecules from the layer below.

The coordination of the other crystallographically identical Mn atoms positioned at both ends of the three-atom chain is less obvious, as it exhibits two relatively short Mn–O bonds [Mn2–O2 2.170(2) Å, Mn2–O10 2.102(4) Å] and one rather long interaction to O1 [Mn2–O1 2.528(2) Å]. This gives a coordination number of either 4 or 7 depending on whether or not the latter bond is included. If all 7 bonds are included the coordination of Mn2 can be described as a capped octahedron. On the other hand, if the long Mn2–O1 bonds are ignored, the Mn2 exhibits a highly distorted tetrahedral coordination to O10 and the three crystallographically equivalent O2 atoms, as the O10–Mn2–O2 angle is 92.11(5)°. It would be of considerable interest to examine the chemical bonding of **1** by using topological analysis of the charge density,[8] but attempts to measure charge density quality data have so far been unsuccessful.

The two aromatic rings of the BPDC linkers in **1** are due to symmetry exactly coplanar, and the carboxylate groups are only slightly rotated (by about 1°) out of this plane. The plane of the BPDC linkers are twisted approximately 24° with respect to the threefold inversion axis through the manganese atoms. Due to the threefold rotation symmetry axis along the Mn chain, the three BPDC linker molecules that form the triangular voids all curl in the same direction

with respect to the chain, resulting in alternating opened and closed cavities as seen from either side of the layer. The DMF solvent molecules that terminate the Mn chains fit into these triangular voids from the "closed" side in the neighboring layer, which result in a stacking of the layers perpendicular to the (001) direction. This is illustrated in Figure 2 where spheres marked by a "+" represent the DMF molecules from the layer above and spheres marked by "–" represent the DMF molecules from the layer below. Presumably no strong chemical bonding is taking place between the layers, and the layers appear to be held together by van der Waals forces. To accommodate the DMF molecules of adjacent layers, the 2D layers in **1** are stacked in an offset manner. This horizontal offset is ca. 8 Å between the neighboring Mn chains. The displacement ellipsoids of C3 and C4 in the BPDC linker have enlarged components perpendicular to the plane of the phenyl ring, suggesting that the magnitude of the twist is slightly variable between different BPDC molecules, or that there is significant population of transverse vibrational modes.[4]

Crystal Structure of 2

The crystal structure of **2** does not, as expected from synthesis, contain diethylformamide (DEF) molecules, but instead formic acid residues are present. The latter originate from the decomposition of the DEF solvent molecule under the harsh conditions in the solvothermal synthesis.[9] The framework consists of layers of manganese atoms, and these layers are internally connected by the carboxylate groups of the BPDC linkers and one formate molecule. The BPDC linker molecules form the connections between the layers creating a 3D framework (Figure 3). There are two crystallographically different BPDC linker molecules in the crystal, which are denoted BPDC1 and BPDC2. The two benzene rings of the BPDC1 linker are almost coplanar, and the O1–C1–O2 carboxylate group of BPDC1 is twisted ca. 15° with respect to the benzene ring. The two benzene rings of BPDC2 are noncoplanar (rotated by about 12°) and also slightly twisted with respect to each other. The carboxylate groups of BPDC2 are in plane with the benzene rings.

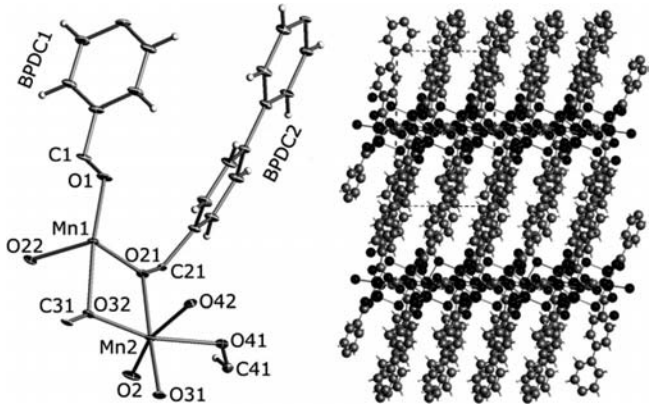

Figure 3. The asymmetric unit of **2**. Thermal ellipsoids are shown at the 50% level (Left). Layered structure viewed along the *b* axis of the unit cell (right).

The layers formed by manganese atoms in the *bc* plane of the unit cell can be divided into separate infinite chains parallel with the *c* axis (Figure 4). Adjacent chains in the layer are connected by the O1–C1–O2 and O21–C21–O22 carboxylate groups of the BPDC1 and BPDC2 linkers, respectively. The carboxylate group of the BPDC1 linker only acts as a linker between the manganese chains within one layer, whereas O21 of BPDC2 besides bridging neighboring chains also acts as a direct oxygen bridge between two Mn atoms within a manganese chain. In a single chain of manganese atoms, the O41–C41–O42 formate group (black dashed bonds in Figure 4) and the O31–C31–O32 carboxylate group (full bonds in Figure 4) constitute the bridges together with O21 (dotted bonds in Figure 4),

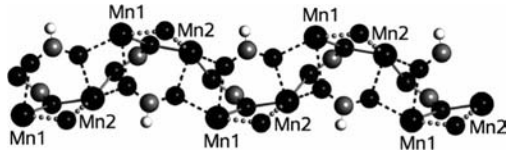

Figure 4. Section of the manganese chain in **2**. Black dashed bonds representing bonds from the formate molecule, full bonds from the O31–C31–O32 carboxylate group and dotted bonds from O21.

Table 2. Bond lengths and bond types in the manganese layers of **2**.

Atom1	Atom2	Bond length [Å]	Type	Type
Mn1	O1	2.096(3)	carboxylate (BPDC1)	interlayer
Mn1	O21	2.155(3)	carboxylate (BPDC2)	direct oxygen bridge
Mn1	O22	2.139(3)	carboxylate (BPDC2)	interlayer
Mn1	O32	2.275(3)	carboxylate (BPDC2)	direct oxygen bridge
Mn1	O41	2.341(3)	formate group	direct oxygen bridge
Mn1	O42	2.216(3)	formate group	direct oxygen bridge
Mn2	O2	2.045(3)	carboxylate (BPDC1)	interlayer
Mn2	O21	2.189(3)	carboxylate (BPDC2)	direct oxygen bridge
Mn2	O31	2.151(3)	carboxylate (BPDC2)	carboxylate
Mn2	O32	2.151(3)	carboxylate (BPDC2)	direct oxygen bridge
Mn2	O41	2.256(3)	formate group	direct oxygen bridge
Mn2	O42	2.184(3)	formate group	direct oxygen bridge

which combines to create both direct oxygen bridges and carboxylate bridges between the manganese atoms of the chain.

The two manganese atoms both have distorted octahedral coordination with angles varying up to 17° from perfect coordination. There are various interaction paths between the magnetic manganese centers in the layers, and the respective distances are listed in Table 2. The differences in the geometry of the two BPDC linkers may originate from their interconnection of the manganese layers. The chains of manganese atoms of adjacent layers are located directly above each other, and hence, there is limited strain in the coplanar BPDC1 linker, which links two neighboring chains. The connectivity of the BPDC2 linker is a little different, as the O31–C31–O32 carboxylate group connects the manganese atoms within a single chain, whereas the other end of this BPDC2 linker, the O21–C21–O22 carboxylate group, joins two manganese chains in the adjacent layer below. It could be speculated that such an arrangement leads to more strain on the BPDC2 linker, resulting in the bent shape of BPDC2.

Crystal Structure of 3

The crystal structure of **3** consists of trimetallic Mn chains coordinated by carboxylate groups of the BPDC linker, thereby creating a 3D framework. The three-membered Mn chains are terminated by direct bonding of two DMA molecules to the terminal Mn1 atom (Figure 5). One of the DMA molecules is disordered in two positions with occupancy of ca. 95% of the most populated site. As in **2**, there are two distinct linkers denoted BPDC1 and BPDC2. In BPDC1, the benzene rings are rotated ca. 39° with respect to each other, and the two unique carboxylate groups are inclined to the benzene ring planes by ca. 10 and 17°. In BPDC2 the benzene rings are, due to symmetry, coplanar but the carboxylate group (O21–C21–O22) is twisted ca. 11° with respect to the aromatic system. All of the carboxylic oxygen atoms coordinate to one manganese atom except O21, which coordinates to both Mn1 and Mn2. This leads to a distorted octahedral coordination around the Mn1 atom with the O21–Mn1–O22 angle being only ca. 59°. The coordination of Mn2 is almost perfectly octahedral. The framework structure of **3** consists of BPDC1 linkers connecting the Mn chains in a "step-like" layer with rhombic voids (Figure 6). Adjacent layers are connected by the BPDC2 linker forming an extended 3D network with rhombic channels along the *c* axis in which the DMA molecules are located.

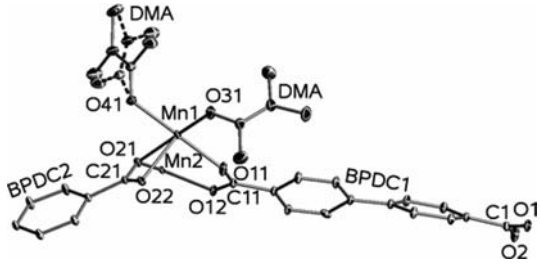

Figure 5. The asymmetric unit of **3**. Dashed bonds in the DMA molecule show the site with ca. 5% occupancy. Hydrogen atoms are omitted for clarity. The thermal ellipsoids are shown at the 50% level.

Physical Properties of 1

The sample batch of **1** is not homogeneous as seen in the powder X-ray diffraction patterns in the Supporting Information (Figure S1). The structure of **1** is the dominant phase, but other peaks are visible in the powder pattern originating from unknown phases. The diffraction pattern measured directly after evaporation of the mother liquid and the pattern of the sample when left for a short period of time is dramatically different. Furthermore, the peaks from **1** are no longer visible in the pattern after prolonged exposure to air. The decomposition of **1** is probably due to either solvent evaporation or structural rearrangement, as earlier observed in zinc coordination polymers.[10] As the sample batch is not phase pure, no measurements of the physical properties were performed.

Physical Properties of 2

Due to the high density of atoms in the framework structure of **2** no cavities are left for storage of the DEF solvent molecules. Thus, the framework is stable, and the solvent-free crystalline material of **2** is not sensitive to air exposure. PXRD analysis revealed that the sample is phase pure, thus enabling measurements of magnetic susceptibility and heat capacity.

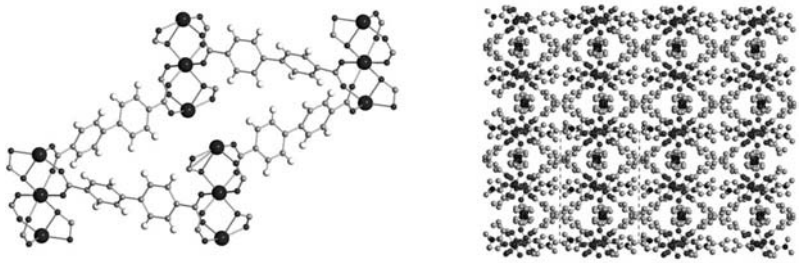

Figure 6. Rhombic voids in **3**. The manganese subchains are connected in a "step-like" layer (left). The 3D network of **3** (right).

Figure 7 shows the inverse magnetic susceptibility (χ^{-1}) of **2** measured between 1.8 and 350 K in a magnetic field (B) of 2.0 T. A fit of the data from 60 to 350 K, excluding the region from 235 to 270 K (shown in light gray), to a Curie–Weiss law gives a Weiss temperature of –23.7(4) K and an effective moment of 6.70(1) μ_B. From the synthesis protocol the manganese ions are expected to have a charge of +2 and as the maximum theoretical value of the effective moment for a spin only Mn^{2+} ion is 5.9 μ_B.[11] The experimentally measured effective moment, μ_{eff}, is somewhat higher than the theoretical value. However, the magnetic susceptibility is a macroscopic property, which does not reveal the detailed atomic origin of the magnetism in the structure, for example, orbital and ligand contributions to the magnetization. Nevertheless, high-spin Mn^{2+} ions are essentially spin-only ions, and it does not seem plausible that the ligands should account for the difference between the experimental finding and the theoretical value. A possible reason for the discrepancy could be a small magnetic impurity possibly introduced into the sample while preparing it for measurement of the magnetization. This could potentially explain the high value of μ_{eff} and the peculiar peak around 245 K. Because we do not know the origin of this peak, we have excluded the region in the Curie–Weiss fit.

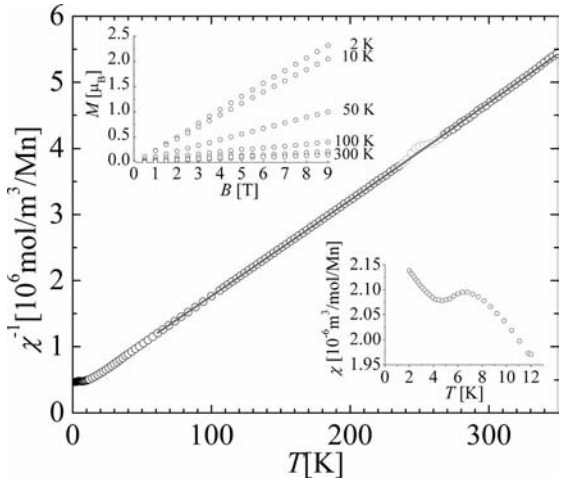

Figure 7. The inverse susceptibility of **2**. The light-gray region around 245 K shows the region excluded in the fit. Upper-left insert shows magnetization at various temperatures. Lower-right insert shows the susceptibility at low temperature.

The lower right inset of Figure 7 shows the low-temperature region, where $\chi(T)$ has a local maximum at approximately 6.5 K. The upper left inset shows a linear magnetization with magnetic field up to 9 T at 2 K. Together with the negative Weiss temperature [Θ = –23.7(4) K] this is an indication of an antiferromagnetic ordering of the manganese atoms below 6.5 K. It is noteworthy, that below the antiferromagnetic ordering temperature, the magnetic susceptibility suddenly changes slope at approximately 4.5 K (Figure 7, lower right inset). The magnetic ordering in the Mn layers is a possible explanation as the Mn atoms in the chains are bridged both directly through a single oxygen atom as well as through formate and carboxylate groups. The ordering between the layers is not as clear as the BPDC linkers are twisted and bent, thereby possibly lacking conjugation through the aromatic system.

Figure 8 shows the heat capacity (C_p) measured between 1.8 and 300 K. Two peaks are clearly present in the low-temperature region with local maxima at approximately 6.5 and 4.5 K, respectively. The first peak at 6.5 K appears as a sharp lambda-type peak in agreement with the antiferromagnetic ordering observed at 6.5 K. The second peak at 4.5 K again is consistent with the change in slope of the magnetic susceptibility. This could indicate that there is a second magnetic ordering. However, the transition could also be a structural transition that leads to a change in slope in the susceptibility. This is based on changes in the X-ray powder diagram, (Figure 9) and the TGA/DTA measured before and after the sample had been cooled to 1.8 K (Figure 10). It is noteworthy that the thermal stability has

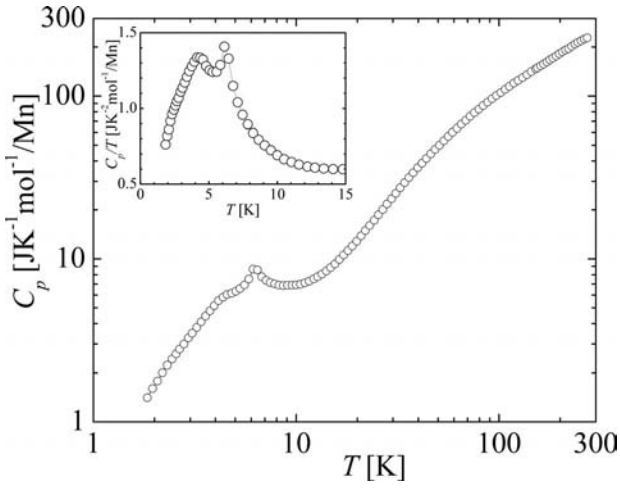

Figure 8. Heat capacity of **2**. Insert shows C_p/T at low temperature.

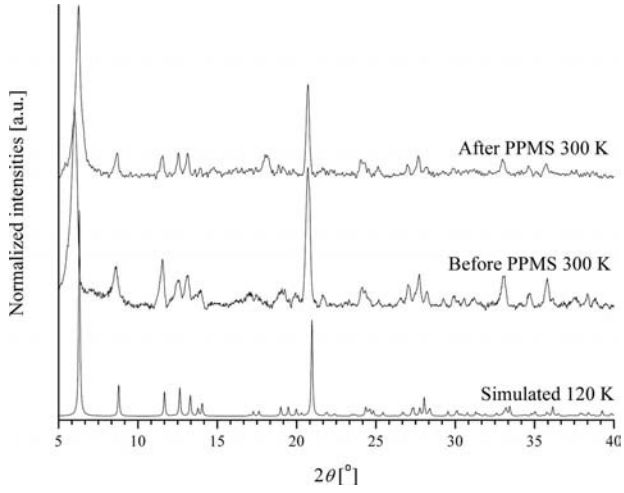

Figure 9. PXRD of **2**. The lower pattern is a theoretical pattern, the middle pattern is measured at 300 K, and the upper pattern is measured after the sample was cooled to 2 K in the PPMS (Physical Properties Measurements System) and reheated to 300 K.

improved significantly after the phase transition (Figure 10). As the phase transition is irreversible a more stable structure is formed, and the structure of **2** must then be metastable. It would be of significant interest to obtain the crystal structure of **2** after the phase transition has occurred. However, as the crystals are minute and very fragile this has not yet been possible even though attempts have been made at high intensity synchrotrons.

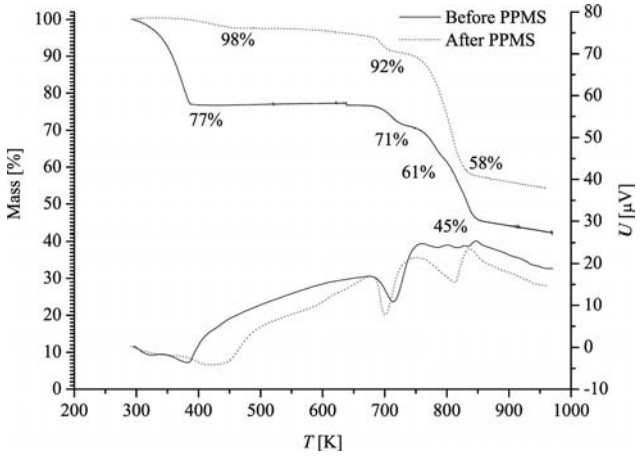

Figure 10. TGA/DSC of **2** before and after cooling to 2 K in the PPMS.

Physical Properties of 3

Visual inspection of the sample batch indicated that it was not homogeneous and that at least two different morphologies were present in the batch. Block-shaped crystals of **3** and very thin and fragile needles of an unknown phase were observed. When powder diffraction data are compared with a theoretical diffraction diagram, it is seen that the dominating phase is indeed **3** but at least one other phase is present (Figure S2). Therefore, measurements of the physical properties were not performed. Several attempts have been made to solve the structure of the needle crystals, but until now only the possible *a* and *b* axes have been determined to ca. 6.49 and 7.38 Å, respectively. The *c* axis remains undetermined due to splitting along the *c* axis.

Conclusions

Solvothermal synthesis in the manganese *p*-biphenyldicarboxylic acid system with variation of solvent molecules resulted in three new coordination polymer structures. The study of compounds **1** and **3** shows that solvothermal synthesis of coordination polymers can produce a variety of products. Product **1** decomposed during exposure to air, demonstrating the risk/possibility of obtaining kinetic metastable products. The structure of **2** elucidates that undesired solvent decomposition is a risk under the harsh solvothermal decomposition. Compound **2** undergoes irreversible phase transition at low temperature to a more stable structure, and hence, the original product of **2** must be thermodynamically metastable. The manganese atoms of the structure of **2** orders antiferromagnetically at a temperature around 6.5 K.

Experimental Section

Synthesis: The synthesis of the three coordination polymers involves a one-pot reaction in small (12 mL) Teflon autoclaves. For **1**, a mixture of *p*-biphenyldicarboxylic acid (H_2BPDC; 0.250 g, 1 mmol) and dimethylformamide (DMF, 8 mL) was added to $Mn(NO_3)_2{\cdot}6H_2O$ (0.293 g, 1 mmol) dissolved in DMF (3 mL). The mixture was kept at 375 K for 40 d. The product was not homogeneous as crystals of different morphology were present. One morphology was colorless rhombic-shaped single crystals of **1**.

A mixture of H_2BPDC (0.250 g, 1 mmol) and diethylformamide (DEF, 8 mL) was added to $Mn(NO_3)$**2**·6H2O (0.293 g, 1 mmol) dissolved in DEF (3 mL). After 40 d at 433 K, minute, needle-shaped, colorless crystals of **2** were formed. The crystals tended to twin, and it was difficult to find a single crystal.

A mixture of H_2BPDC (0.250 g, 1 mmol) and dimethyl amide (DMA, 10 mL) was added to $Mn(NO_3)_2{\cdot}6H_2O$ (0.293 g, 1 mmol) dissolved in DMA (2 mL). The mixture was kept at 434 K for 20 d, and the product formed was not homogeneous. The crystals formed were both block-shaped and needle-like colorless crystals. A block-shaped crystal of **3** was isolated; however, it was not possible to locate a single crystal of the phase with needle-shaped crystals as these are very fragile.

X-ray Crystallography: For **1** and **3**, colorless crystals ($0.100 \times 0.100 \times 0.150$ mm and $0.100 \times 0.125 \times 0.150$ mm, respectively) were mounted in protective oil on a glass fiber rod glued to a small copper wire. This assembly was mounted on a brass pin, which was placed on the goniometer of a SMART 1 K diffractometer at the Department of Chemistry, Aarhus University. The experiments were carried out at 293 and 100 K, respectively through an ω- and ϕ-scan experiment by using a step width of 0.3°. All data reduction and structure solution were performed with the Bruker SMART suite of programs.[12]

For **2**, a minute, colorless crystal ($0.040 \times 0.030 \times 0.140$ mm) was mounted by using protective oil in a loop. This was mounted on a brass pin, which was placed on the goniometer of a 6-circle Kuma diffractometer at the Swiss-Norwegian Beamline at ESRF, Grenoble, equipped with an Oxford CCD detector system. The data collection was carried out at beamline BM01A at a wavelength of 0.71 Å obtained from a double Si(111) crystal monochromator. The temperature was kept at 120(1) K by using an Oxford Nitrogen Cryostream. The ω-scan experiment used a step width of 1.0° at two different κ settings. Data were integrated with CryAlis RED.[13] The data were corrected for absorption by using a spherical correction included in the WinGX program package.[14] Structure solution was performed by using the SHELX program package.[15]

Measurement of Physical Properties: Measurements of the magnetic susceptibility, χ, and total heat capacity (C_p) of **2** were performed with a Quantum Design Physical Properties Measurements System (PPMS) at the Department of Chemistry, Aarhus University, Denmark, on pellets pressed from finely ground powder. The purity of the bulk samples was examined with conventional powder X-ray diffraction data measured with a STOE diffractometer at the Department of Chemistry, Aarhus University, Denmark, by using Cu-$K_{\alpha 1}$ radiation from a curved Ge(111) monochromator and a position sensitive detector covering 40° in 2θ.

The thermal stability of **2** was examined by simultaneous Thermo Gravimetric Analysis (TGA) and Differential Thermal Analysis (DTA). The experiments were carried out by using a Stanton-Redcroft TGA-DTA simultaneous thermal analyzer STA 1000/1500 at the Department of Chemistry, Aarhus University, Denmark. A heating rate of 10 °C/min was applied in an argon gas flow.

CCDC-701624 (for **1**), -701625 (for **2**), -701626 (for **3**) contain the supplementary crystallographic data for this paper. These data can be obtained free of charge from The Cambridge Crystallographic Data Centre via www.ccdc.cam.ac.uk/data_request/cif.

Supporting Information (see footnote on the first page of this article): Powder X-ray diffraction patterns of **1** and **3**.

Acknowledgments

The work was supported by the Danish Strategic Research Council (Centre for Energy Materials) and the Danish National Research Foundation (Center for Materials Crystallography). Beam time at the Swiss–Norwegian Beamlines (SNBL) at the European Synchrotron Radiation Facility (ESRF) is gratefully acknowledged.

[1] a) B. L. Chen, S. C. Xiang, G. D. Qian, *Acc. Chem. Res.* **2010**, *43*, 1115–1124; b) H. X. Deng, C. J. Doonan, H. Furukava, R. B. Ferreira, J. Towne, C. B. Knobler, B. Wang, O. M. Yaghi, *Science* **2010**, *327*, 846–850; c) O. K. Farah, J. T. Hupp, *Acc. Chem. Res.* **2010**, *43*, 1166–1175; d) H. Furukawa, J. Kim, N. W. Ockwig, M. O'Keeffe, O. M. Yaghi, *J. Am. Chem. Soc.* **2008**, *130*, 11650–11661; e) H. Furukawa, N. Ko, Y. B. Go, N. Aratani, S. B. Choi, E. Choi, A. O. Yazaydin, R. Q. Snurr, M. O'Keeffe, J. Kim, O. M. Yaghi, *Science* **2010**, *329*, 424–428; f) S. S. Kaye, A. Dailly, O. M. Yaghi, J. R. Long, *J. Am. Chem. Soc.* **2007**, *129*, 14176–14177; g) J. L. C. Roswell, O. M. Yaghi, *Microporous Mesoporous Mater.* **2004**, *73*, 3–14; h) S. L. Qui, G. S. Zhu, *Coord. Chem. Rev.* **2009**, *253*, 2891–2911; i) Z. Q. Wang, S. M. Cohen, *Chem. Soc. Rev.* **2009**, *38*, 1315–1329; j) A. G. Wong-Foy, A. J. Matzger, O. M. Yaghi, *J. Am. Chem. Soc.* **2006**, *128*, 3494–3495; k) W. Zhou, *Chem. Rec.* **2010**, *10*, 200–204.

[2] a) D. Britt, C. Lee, F. J. Uribe-Rhomo, H. Furukawa, O. M. Yaghi, *Inorg. Chem.* **2010**, *49*, 6387–6389; b) I. Isaeva, L. M. Kustov, *Petrol. Chem.* **2010**, *50*, 167–180; c) J. Lee, O. K. Farah, J. Roberts, K. A. Scheidt, S. T. Nguyen, J. T. Hupp, *Chem. Soc. Rev.* **2009**, *38*, 1450–1459; d) VK, L. Lim, H. Kazemian, Z. Yaakob, W. R. W. Daud, *Chem. Eng. Technol.* **2010**, *33*, 213–226; e) K. Oisaki, Q. W. Li, H. Furukawa, A. U. Czaja, O. M. Yaghi, *J. Am. Chem. Soc.* **2010**, *132*, 9262–9264; f) N. T. S. Phan, K. K. A. Le, T. D. Phan, *Appl. Catal. A* **2010**, *382*, 246–253.

[3] a) D. Britt, H. Furukawa, B. Wang, T. G. Glover, O. M. Yaghi, *Proc. Natl. Acad. Sci. USA* **2009**, *106*, 20637–20640; b) D. Britt, D. Tranchemontagne, O. M. Yaghi, *Proc. Natl. Acad. Sci. USA* **2008**, *105*, 11623–11627; c) J. R. Li, R. J. Kuppler, H. C. Zhou, *Chem. Soc. Rev.* **2009**, *38*, 1477–1504; d) K. S. Walton, A. R. Millward, D. Dubbeldam, H. Frost, J. J. Low, O. M. Yaghi, R. Q. Snurr, *J. Am. Chem. Soc.* **2008**, *130*, 406–407; e) R. Q. Zou, A. I. Abdel-Fattah, H. W. Xu, Y. S. Zhao, D. D. Hickmott, *CrystEngComm* **2010**, *12*, 1337–1353.

[4] a) A. Y. Robin, K. M. Fromm, *Coord. Chem. Rev.* **2006**, *250*, 2127–2157; b) S. Kitagawa, R. Kitaura, S.-I. Noro, *Angew. Chem.* **2004**, *116*, 2388; *Angew. Chem. Int. Ed.* **2004**, *43*, 2334–2375; c) Y. Wu, A. Kobayashi, G. J. Halder, V. K. Peterson, K. W. Chapman, N. Lock, P. D. Southon, C. J. Kepert, *Angew. Chem.* **2008**, *120*, 9061; *Angew. Chem. Int. Ed.* **2008**, *47*, 8929–8932; d) N. Lock, Y. Wu, M. Christensen, L. J. Cameron, V. K. Peterson, A. J. Bridgeman, C. J. Kepert, B. B. Iversen, *J. Phys. Chem. C* **2010**, *114*, 16181–16186.

[5] a) H. F. Clausen, J. Overgaard, Y.-S. Chen, B. B. Iversen, *J. Am. Chem. Soc.* **2008**, *130*, 7988–7996; b) R. D. Poulsen, M. R. V. Jørgensen, J. Overgaard, F. K. Larsen, W. Morgenroth, T. Graber, Y.-S. Chen, B. B. Iversen, *Chem. Eur. J.* **2007**, *13*, 9775–9790.

[6] a) R. D. Poulsen, A. Bentien, M. Chevalier, B. B. Iversen, *J. Am. Chem. Soc.* **2005**, *127*, 9156–9166; b) R. D. Poulsen, A. Bentien, T. Graber, B. B. Iversen, *Acta Crystallogr., Sect. A* **2004**, *60*, 382–389.

[7] C.-B. Ma, C.-N. Chen, Q.-T. Liu, *CrystEngComm* **2005**, *7*, 650–655.

[8] R. F. W. Bader, *Atoms in Molecules – A Quantum Theory*, Oxford University Press, Oxford, **1990**.

[9] T. H. Lowery, K. S. Richardson, *Mechanism and Theory in Organic Chemistry*, 3rd ed., Harper & Row, New York, **1987**.

[10] H. F. Clausen, R. D. Poulsen, A. D. Bond, M.-A. S. Chevallier, B. B. Iversen, *J. Solid State Chem.* **2005**, *11*, 3342–3351.

[11] N. W. Ashcroft, N. D. Mermin, *Solid State Physics*, Brooks Cole, London, **1976**.

[12] SAINT+, SADABS, *SHELXTL*; SMART, Bruker AXS Inc., Madison, WI, **1998**.

[13] *CryAlis RED*, Oxford Diffraction, **2004**.

[14] L. J. Farrugia, *J. Appl. Crystallogr.* **1999**, *32*, 837–838.

[15] G. M. Sheldrick, *Acta Crystallogr., Sect. A* **2008**, *64*, 112–122.

Received: September 19, 2010
Published Online: December 28, 2010

